Available online at www.sciencedirect.com

ScienceDirect

Ceramics International 40 (2014) 2315–2322

CERAMICS INTERNATIONAL

www.elsevier.com/locate/ceramint

Compressive mechanical properties of porous alumina powder compacts

Yoshihiro Hirata*, Taro Shimonosono, Tatsuoki Sameshima, Soichiro Sameshima

Department of Chemistry, Biotechnology, and Chemical Engineering, Kagoshima University, 1-21-40 Korimoto, Kagoshima 890-0065, Japan

Received 4 July 2013; received in revised form 26 July 2013; accepted 31 July 2013
Available online 7 August 2013

Abstract

In this study, compressive mechanical properties, relative density, porosity, grain size, and grain boundary area of porous alumina ceramics, were examined at room temperature to clarify the influence of microstructures. High purity alumina powder of median size 150 nm was dispersed in an aqueous solution at pH 3.0 and consolidated by pressure filtration to achieve a uniform microstructure. The grain boundary development was analyzed using an initial sintering model and the decreased Brunauer–Emmett–Teller specific surface area during sintering. When the alumina compacts were sintered at 500–1400 °C, the relative density (60.2–62.9%) was almost constant up to 1000 °C, while the specific surface area decreased above 800 °C. The Young's modulus and compressive strength of porous alumina compacts increased exponentially with sintering temperature. The abovementioned mechanical properties were well explained by the increased grain boundary area during sintering. Another factor that contributes to the observed increase in the mechanical strength of porous alumina compacts is the increase in packing density, leading to an increase in the total grain boundary area. An effective compressive strength (830 MPa) for dense alumina compacts of 0% porosity was estimated from the relationship between measured compressive strength and grain boundary area, which was 1/4–1/3 times that of the compressive strength reported for dense alumina materials.

Keywords: B. Grain boundaries; B. Porosity; C. Strength; D. Al_2O_3

1. Introduction

Porous ceramics are used in various applications, such as thermal insulators, separation membranes, catalyst supports, and electrodes for solid oxide fuel cells, because of their high stability against chemical reaction, heat shock, and mechanical stress. Recently, our group developed an electrochemical cell composed of porous electrodes and a porous electrolyte to generate hydrogen fuel through methane reforming with carbon dioxide without carbon deposition ($CH_4+CO_2 \rightarrow 2H_2+2CO$) [1–3]. In the electrochemical cell, a thermal stress is induced in the cathode and anode owing to the endothermic reduction reaction ($CO_2+2e^- \rightarrow CO+O^{2-}$) and exothermic oxidation reaction ($CH_4+O^{2-} \rightarrow 2H_2+CO+2e^-$), respectively. Therefore, we anticipate that the improvement in mechanical properties will enable the use of porous ceramics under more severe conditions.

The mechanical properties of porous ceramics have been experimentally formulized as a function of porosity in the 1950–1960s, as reviewed in a handbook [4]. Accordingly, the empirical relationship is given by Eq. (1):

$$\sigma = \sigma_0 \exp(-\beta\varepsilon), \quad (1)$$

where σ and σ_0 are the strengths of ceramics with and without pores, respectively, β is the parameter determined by the nature of porosity, and ε is the porosity. According to the above-mentioned relationship, depending on the β value, the strength of porous ceramics decreases nonlinearly with porosity. For instance, it was reported that the mechanical properties of porous alumina sintered at 1860 °C, where alumina grains are strongly connected, decrease with increase in porosity [5].

Typically, a lower sintering temperature is expected to save energy and cost associated with the fabrication of porous ceramics. In the 1980–1990s, there were some attempts to relate the

*Corresponding author. Tel.: +81 99 285 8325; fax: +81 99 257 4742.
E-mail address: hirata@apc.kagoshima-u.ac.jp (Y. Hirata).

0272-8842/$ - see front matter © 2013 Elsevier Ltd and Techna Group S.r.l. All rights reserved.
http://dx.doi.org/10.1016/j.ceramint.2013.07.153

mechanical properties of porous ceramics with the microstructure of solid phase, such as the developed grain boundary, coordination number of grains, and solid phase contiguity [6–9]. For example, Green et al. proposed that the bulk modulus of partially sintered glass spheres is proportional to the coordination number of glass spheres and the ratio of the grain boundary to sphere radius [6,7,10]. Similarly, Hardy and Green experimentally reported a drastic improvement in the mechanical properties at the initial stages of sintering, which was attributed to the grain boundary development between coalesced particles [11]. We believe that a comprehensive understanding of the factors determining the mechanical properties of porous ceramics is necessary for application.

Therefore, in this study, we have quantitatively clarified the crucial factors that determine the mechanical properties of porous ceramics by measuring the specific surface area, grain size, porosity, Young's modulus, and compressive strength of porous alumina ceramics sintered at low temperatures. As a presintering step, the fine alumina particles in a colloidal suspension were consolidated by high-pressure filtration to achieve alumina powder compacts with a uniform microstructure. On the basis of the experimental results, a model relating the coordination number of grains and grain boundary area with compressive strength has been developed.

2. Experimental

Fig. 1 shows the experiment flowchart. Porous alumina ceramics was fabricated using α-Al_2O_3 powder (specific surface area 10.21 m^2/g, equivalent diameter 150 nm, Al_2O_3 purity > 99.99 mass%; AKP-50, Sumitomo Chemical Co. Ltd., Japan). The alumina powder (isoelectric point of pH 8.5) was dispersed at a solid content of 15 vol% in an aqueous solution at pH 3.0. The positively charged alumina particles (zeta potential 45 mV) were uniformly dispersed in the suspension because of the strong repulsive energy between them. After stirring for 24 h, the suspension was consolidated using a pressure filtration apparatus

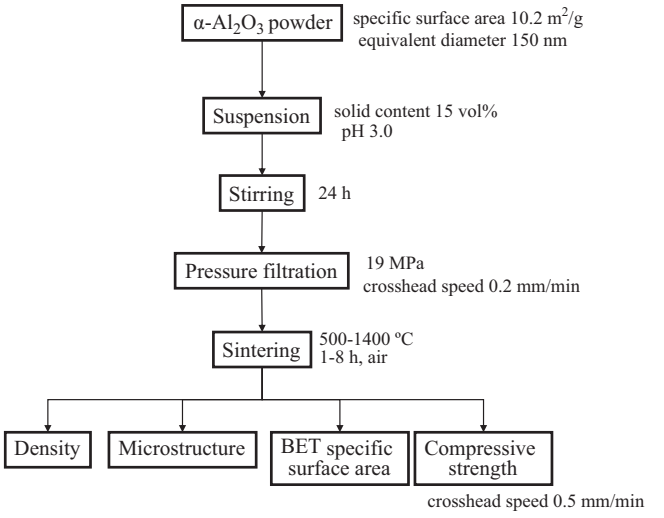

Fig. 1. Flowchart of the fabrication and mechanical test of porous alumina compacts.

[12,13] at a constant crosshead speed of 0.2 mm/min up to 19 MPa. The filtrate was exhausted from the upper side using a three-layered membrane filter of pore size 0.1 μm. The resulting consolidated powder cake was dried at 100 °C in air for 24 h, and then sintered at 500–1400 °C for 1–8 h.

The bulk and apparent densities of sintered alumina compacts were measured using the Archimedes method in distilled water. The Brunauer–Emmett–Teller (BET) specific surface area of the alumina compacts was also measured using a fluid-type specific-surface-area auto measurement apparatus (FlowSorb II 2300, Shimadzu Co., Japan). Furthermore, microstructures were observed using a field emission scanning electron microscope (FE-SEM, S-4100H, Hitachi High-Technologies Co., Japan). Fig. 2 illustrates the schematic of the compressive test adopted in this study. The sample was sandwiched between two laminates composed of copper-plate ($20 \times 20 \times 1$ mm^3)–sintered-SiC-plate ($20 \times 18 \times 7$ mm^3)–copper-plate ($20 \times 20 \times 1$ mm^3). Subsequently, the sample was compressed at a crosshead speed of 0.5 mm/min, while the strain was measured along the compression direction using a strain gauge attached to the sample. The compressive test was repeated four times for each sample.

3. Results and discussion

3.1. Sintering behavior

Fig. 3(a) shows the relative density and decrease in the specific surface area of the alumina compacts, prepared from the standard raw powder, as a function of sintering temperature. These structural parameters were well reproduced, as shown by the error bars in Fig. 3(a). This indicates that pressure filtration enables the preparation of alumina powder compacts with a uniform microstructure. As evidenced from the figure, the increase in the relative density (60.5–62.9%) was negligible up to a sintering temperature of 1000 °C for 1 h. The apparent densification occurred above 1000 °C. The decrease in the specific surface area was less than 1 m^2/g at 500–700 °C, while that at 800 and 1000 °C were 1.26 and 3.82 m^2/g, respectively. This implies that the specific surface area decreased without an apparent change in densification at 800–1000 °C. The mechanical properties of the sample shown in Fig. 3(b) are described in the subsequent section.

Fig. 4 shows the microstructures of alumina compacts sintered at different temperatures. No distinguishable changes

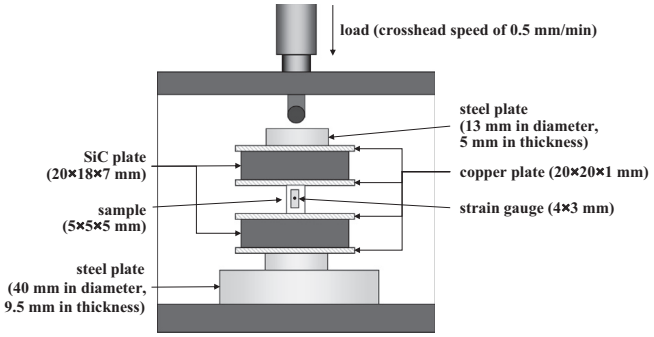

Fig. 2. Schematic of the compressive test of the porous alumina compacts.

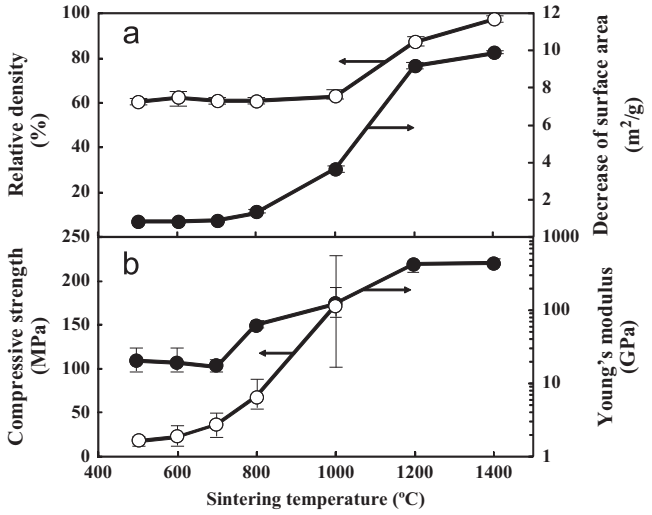

Fig. 3. (a) Relative density and decrease in specific surface area and (b) Young's modulus and compressive strength as a function of sintering temperature.

in the microstructures were observed for samples sintered at 500–1000 °C. On the other hand, the microstructure of alumina compacts sintered at 1200 °C was characterized by faceting and coarsening of grains, in accordance with the densification observed at 1200 °C (Fig. 3(a)). Fig. 5 shows the cumulative distributions of grain sizes, as analyzed from the microstructures shown in Fig. 4. The measured grain sizes were fitted well by normal distribution curves. The median sizes were almost constant up to 800 °C, while they slightly increased at 1000 °C, and by a factor of approximately 2 at 1200 °C. The above measurements indicate that no significant increase in the relative density occurred at 500–1000 °C, while the change in the microstructures (grain growth and decrease in specific surface area) became apparent above 1000 °C.

Fig. 6(a) shows the relative density and decrease in the specific surface area of the alumina compacts sintered at 700 °C, plotted as a function of sintering time. While the relative density (60.2–62.1%) was independent of sintering time, the specific surface

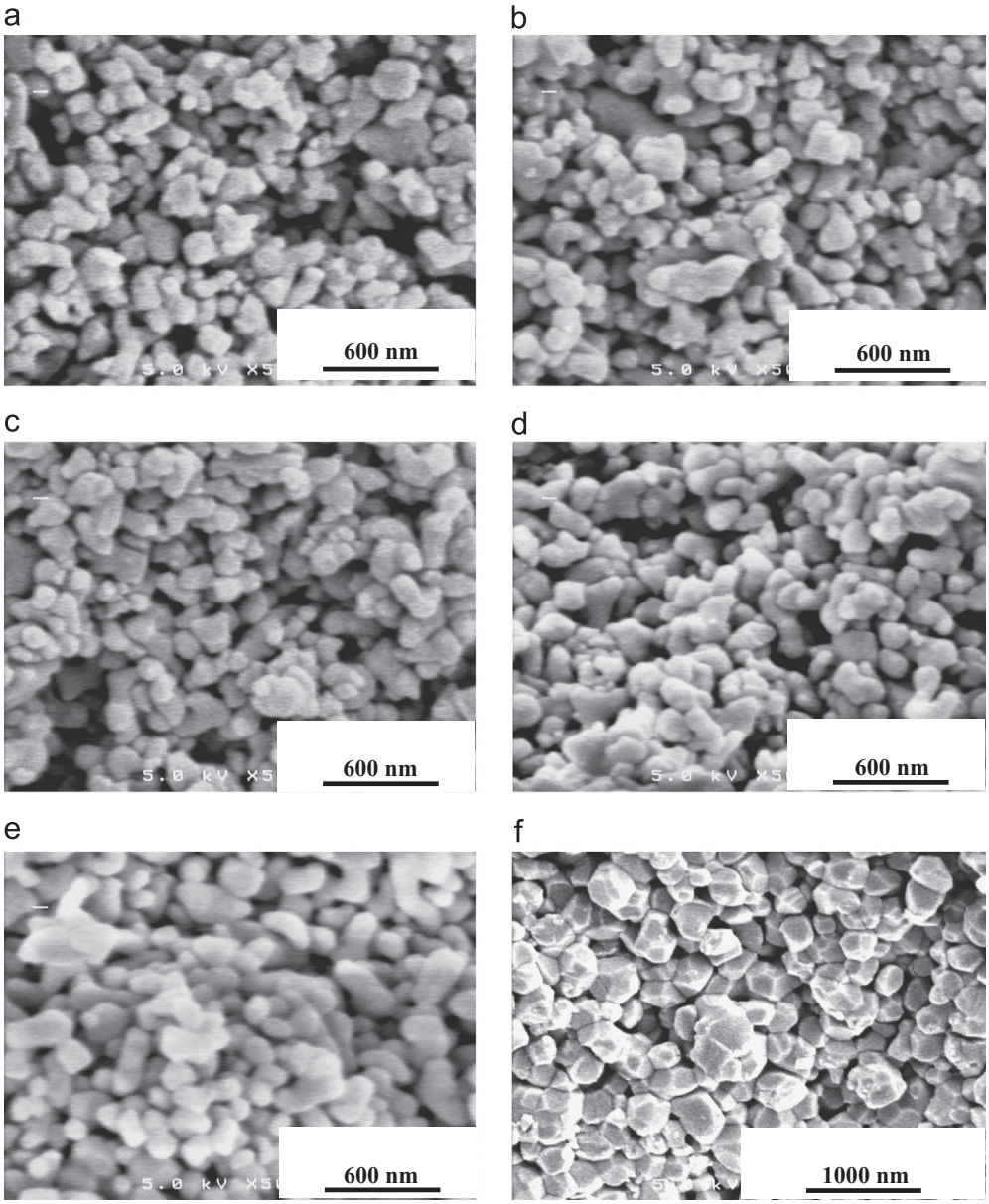

Fig. 4. Microstructures of the alumina compacts sintered at (a) 500 °C, (b) 600 °C, (c) 700 °C, (d) 800 °C, (e) 1000 °C, and (f) 1200 °C.

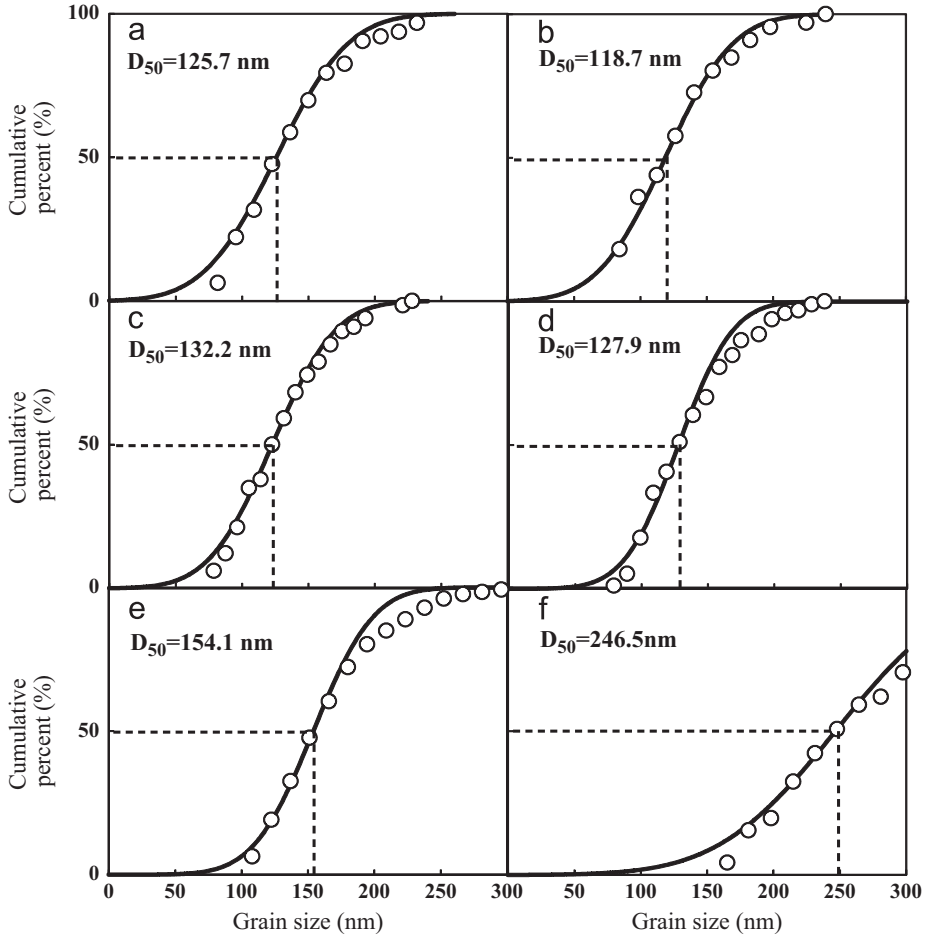

Fig. 5. Cumulative grain size distribution in alumina compacts sintered at (a) 500 °C, (b) 600 °C, (c) 700 °C, (d) 800 °C, (e) 1000 °C, and (f) 1200 °C.

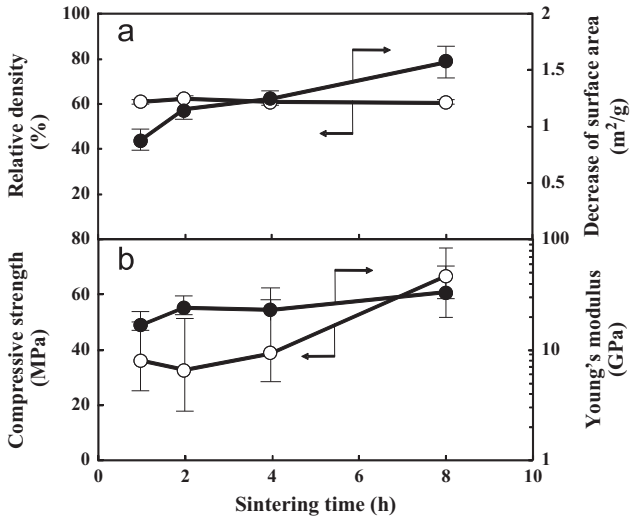

Fig. 6. (a) Relative density and decrease in specific surface area and (b) Young's modulus and compressive strength of alumina compacts as a function of sintering time at 700 °C.

area showed a slight decrease with increasing sintering time. The mechanical properties of the samples, discussed in Fig. 6(b), are described in the next section. Fig. 7 shows the microstructural change of alumina compacts with sintering time. The grain size distributions also fitted well by normal distribution curves. As evidenced from the microstructural analysis, negligible grain growth was observed at 700 °C. The median sizes of the compacts sintered at 700 °C for 1, 2, 4, and 8 h were 132, 123, 158, and 141 nm, respectively.

3.2. Compressive mechanical properties

Fig. 8 shows the relationship between compressive stress and strain for the alumina compacts sintered at different temperatures. The compressive strength could not be measured for alumina compacts sintered at 1200 and 1400 °C because the compressive stress approached 200 MPa, which corresponded to the maximum mechanical loading (5 kN) of the equipment. In case of alumina compacts sintered at 1200 and 1400 °C, the compressive stress increased significantly even for a small strain. On the other hand, nonlinear and sometimes zigzag-like deformation of the stress–strain curve was observed for porous alumina compacts sintered at 500–1000 °C. Such a nonlinear deformation behavior can be attributed to the wide distribution of strengths at the grain boundaries as well as the stress concentration and stress relaxation at different grain boundaries occurring simultaneously. The propagation of cracks, which originate from the weaker and tensile- or shear-stress-concentrated grain boundary, stops at the grain boundary with high compressive strength. As the stress

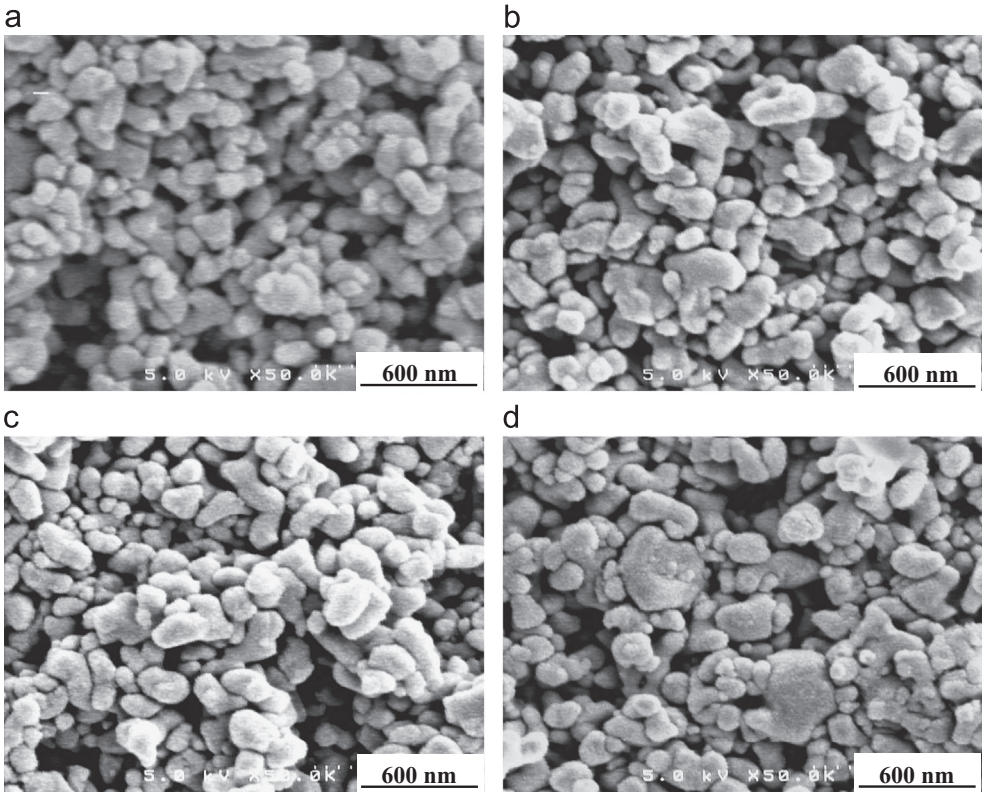

Fig. 7. Microstructures of porous alumina compacts sintered at 700 °C for (a) 1, (b) 2, (c) 4, and (d) 8 h.

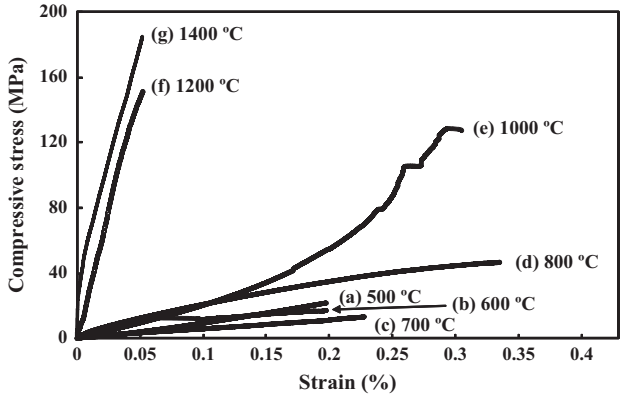

Fig. 8. Relationship between compressive stress and strain for alumina compacts sintered at different temperatures.

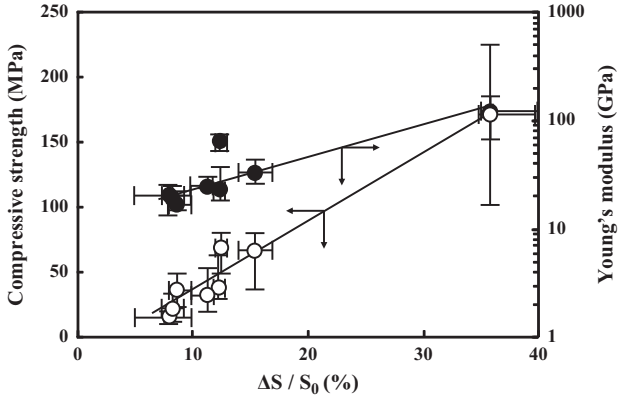

Fig. 9. Influence of decrease in specific surface area on Young's modulus and compressive strength of alumina compacts sintered at 500–1000 °C for 1–8 h.

increases, the formation, propagation, and inhibition of cracks occur repeatedly.

Fig. 3(b) summarizes the Young's modulus and compressive strength of alumina compacts sintered at different temperatures. The Young's modulus was measured from the slope of the stress–strain curves, shown in Fig. 8, below 0.05% strain. The Young's modulus increased above a sintering temperature of 800 °C and reached a constant value (427–454 GPa) at 1200–1400 °C. Also, the compressive strength increased exponentially with increase in sintering temperature. Such a trend of mechanical properties on sintering temperature is not explained by the relative density at 500–1000 °C (Fig. 3(a)); however, this trend is similar to the decrease in specific surface

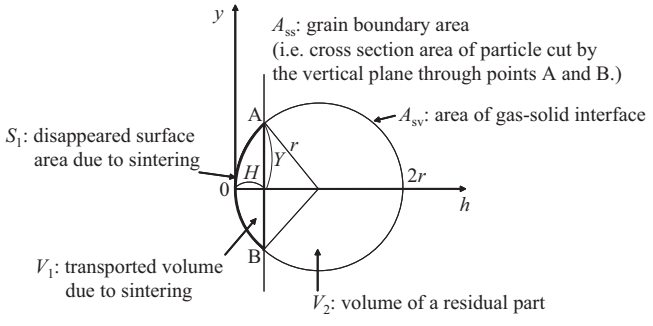

Fig. 10. Schematic of the grain boundary development.

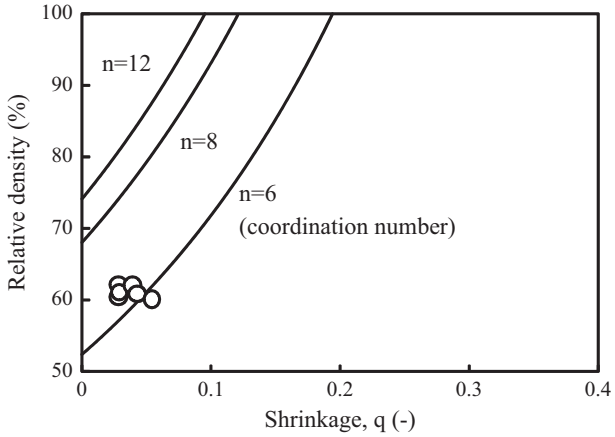

Fig. 11. Comparison of shrinkages between the values calculated by Eq. (12) (solid lines) and those measured experimentally by Eq. (13) (circle plot) as a function of relative density for alumina compacts sintered at 500–800 °C for 1–8 h.

area with increase in sintering temperature (Fig. 3(a)). The stress–strain curves of alumina compacts sintered at 700 °C for various times showed a similar nonlinear relationship.

Fig. 6(b) shows the Young's modulus and compressive strength as a function of sintering time at 700 °C. The mechanical properties increased with sintering time at a similar relative density. This trend is again similar to the decrease in specific surface area, as observed in Fig. 6(a). Fig. 9 shows the influence of decreased specific surface area on the Young's modulus and compressive strength of porous alumina compacts sintered at 500–1000 °C for 1–8 h. The compressive strength linearly increased with decrease in specific surface area, while the Young's modulus exponentially increased at a similar relative density (60.2–62.8%). The results in Fig. 9 are closely related to the grain boundary development between alumina grains, which will be discussed in the following section.

3.3. Calculation of grain boundary area and its influence on mechanical properties

Fig. 10 shows the model structure used for the calculation of the grain boundary area at the initial stages of sintering. The transverse axis (h-axis) represents the distance from the particle surface to particle center. The longitudinal axis (y-axis) represents the line tangent to the particle surface. When one particle is adhered to an adjacent particle by sintering, a grain boundary is formed between the two particles, which is shown by line A–B. The volume V_1 transported to an adjacent particle by sintering is expressed by Eq. (2):

$$V_1 = \int_0^H \pi(2hr - h^2)\, dh = \pi\left(rH^2 - \frac{H^3}{3}\right), \tag{2}$$

where r is the particle radius after sintering. Also, the residual volume V_2 is expressed by Eq. (3):

$$V_2 = \frac{4}{3}\pi r^3 - nV_1, \tag{3}$$

where n is the coordination number of the particles. On substituting Eq. (2) for V_1 in Eq. (3), we get Eq. (4):

$$V_2 = \frac{\pi r^3}{3}(4 - 3np^2 + np^3), \tag{4}$$

where p is the ratio of H to r. Assuming constant volume and constant particle number before and after sintering, V_2 in Eq. (4) is equal to the volume of the starting particle before sintering. The above relationship provides Eq. (5):

$$r = r_0\left(\frac{4}{4 - 3np^2 + np^3}\right)^{1/3}, \tag{5}$$

where r_0 is the starting particle radius before sintering. The equation shows the dependence of particle radius on p and n values during sintering. Furthermore, the surface area S_1 disappears after sintering and is expressed by Eq. (6):

$$S_1 = 2\pi rH \tag{6}$$

Then, the residual surface area A_{SV} is expressed by Eq. (7):

$$A_{SV} = 4\pi r^2 - nS_1 \tag{7}$$

Substituting Eq. (6) for S_1 in Eq. (7) provides Eq. (8):

$$A_{SV} = 2\pi\, r^2(2 - np) \tag{8}$$

The r value in Eq. (8) is substituted by Eq. (5), resulting in Eq. (9):

$$A_{SV} = 4^{2/3}\pi r_0^2 \frac{4 - 2np}{(4 - 3np^2 + np^3)^{2/3}} \tag{9}$$

The p value can be calculated by measuring the decrease in specific surface area (ΔA_{SV}) of the alumina compacts and by assuming a coordination number. Furthermore, the grain boundary area (A_{SS}) is expressed by Eq. (10) as a function of p value:

$$A_{SS} = \frac{1}{2}n\pi\, Y^2 = \frac{1}{2}n\pi\left[r^2 - (r - H)^2\right] = 2^{1/3}\pi r_0^2 n \frac{2p - p^2}{(4 - 3np^2 + np^3)^{2/3}} \tag{10}$$

When estimating the coordination number of particles, we can calculate the grain boundary area using Eq. (10) under constant total grain number and coordination number before and after sintering.

The linear shrinkage (q), defined by Eq. (11), is calculated from the relative density, expressed by Eq. (12), and shown as solid lines in Fig. 11.

$$q = \frac{H}{r_0}, \tag{11}$$

$$D = \left(\frac{1}{1 - q}\right)^3 D_0, \tag{12}$$

where D_0 and D are the relative densities of green and sintered compacts, respectively. The relative density depends on the coordination number of packed particles. The coordination numbers of particles (n) in simple, body-centered, and face-centered cubic structures are 6, 8, and 12, respectively, while the relative densities (D_0) are 0.52, 0.68, and 0.74, respectively.

On the other hand, the q/p ratio is given by Eq. (13):

$$\frac{q}{p} = \frac{r}{r_0} = \left(\frac{4}{4-3np^2+np^3}\right)^{1/3} \quad (13)$$

Since the p value is experimentally determined from Eq. (9) at a given n value and the measured specific surface area, it is substituted in Eq. (13) to obtain the q value. The q values determined from Eq. (13) at $n=6$ for alumina compacts sintered at 500–800 °C for 1–8 h are plotted against the measured relative densities, as shown in Fig. 11. These data were very close to the theoretical curve derived from Eq. (12) at $n=6$. The observed agreement in the q values determined from Eqs. (12) and (13) suggests that the coordination number 6 is valid during the initial stages of sintering for green compacts of 60% relative density.

Fig. 12(a) illustrates the schematic of the grain boundary development at the coordination number 6. The powder compacts show a simple cubic structure, with the shaded area representing the grain boundary area. Fig. 12(b) shows the sintering temperature dependence of grain boundary diameter (R) and p value at $n=6$ for alumina compacts sintered at 500–1400 °C for 1 h. The grain boundary diameter is expressed using the p value by Eq. (14):

$$\begin{aligned} R &= 2Y \\ &= 2\sqrt{r^2-(r-H)^2} \\ &= 2^{5/3} r_0 \sqrt{\frac{2p-p^2}{(4-3np^2+np^3)^{2/3}}} \end{aligned} \quad (14)$$

The grain boundary diameter and the p value showed a similar tendency on sintering temperature. That is, a rapid increase of R and p values occurred above 800 °C; these values were then saturated at 1200–1400 °C. The measured compressive strength is determined by Eq. (15):

$$\sigma = \frac{F}{L^2} = \frac{\sigma_0 \pi (R/2)^2 N^{2/3}}{L^2}, \quad (15)$$

where F and L^2 are the mechanical load and apparent area of the compressed alumina compacts, respectively. The compressive load is applied to the total grain boundary area ($\pi(R/2)^2N^{2/3}$) in Fig. 12 (a), where N is the particle number of the cubic powder compacts. When the compressive strength at 0% porosity is constant (σ_0, effective compressive strength), the measured strength is related to the right-hand term of Eq. (15). Fig. 13 shows the relationship between the measured strength and $\pi(R/2)^2N^{2/3}/L^2$ value for alumina compacts sintered at 500–1000 °C for 1–8 h. As

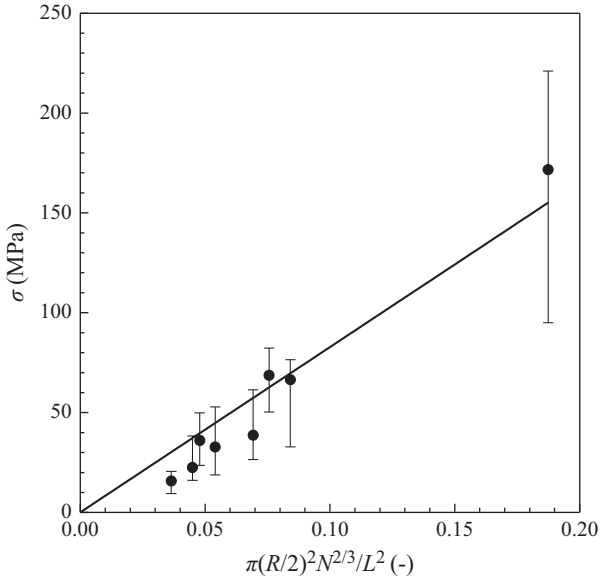

Fig. 13. Relationship between measured compressive strength and grain boundary area calculated by Eq. (15) for alumina compacts sintered at 500–1000 °C for 1–8 h.

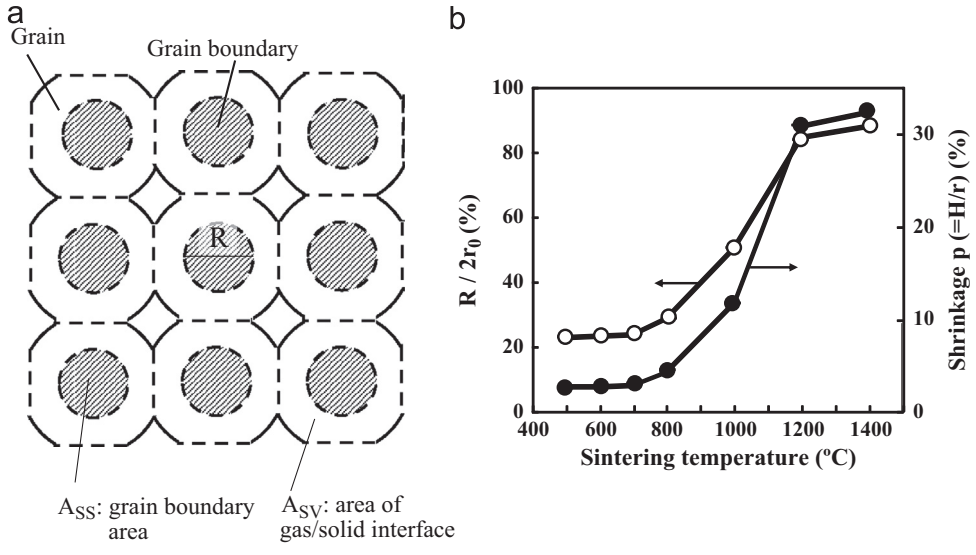

Fig. 12. Schematic of (a) the grain boundary formation and (b) variation of grain boundary diameter (R) and shrinkage (p) with sintering temperature for the coordination number 6 of alumina compacts sintered at 500–1400 °C for 1 h.

seen in Fig. 13, the compressive strength increased with the grain boundary area. That is, the increases in particle number (N) packed in powder compacts and the grain boundary area ($\pi R^2/4$) are the key factors contributing to the increase in compressive strength of porous powder compacts. The σ_0 value, determined from the straight line slope in Fig. 13, was found to be 827 MPa, which was almost 1/4–1/3 times the compressive strength (2.2–3.3 GPa) of dense alumina ceramics [5,14]. This result may reflect the formation of weak chemical bonds at the grain boundaries at low sintering temperatures, which will be analyzed in detail in our future work.

4. Conclusions

In this study, the compressive strength of porous alumina powder compacts was examined to clarify the influence of mechanical properties on the grain boundary development at the initial stages of sintering. The specific surface area analysis reflected the negligible microstructural changes during grain boundary development. The Young's modulus and compressive strength of alumina compacts with relative densities of 60.2–62.9% increased with sintering temperature from 500 to 1000 °C. This result was explained by the increase in the grain boundary area, which was determined from the decrease in specific surface area. Another factor that contributes to the increase in compressive strength while maintaining high porosity is the increase in packing density, leading to an increase in the total grain boundary area in powder compacts. The effective compressive strength corresponding to dense alumina of 0% porosity, which was determined from the relationship between grain boundary area and measured strength, was found to be 827 MPa. This value was 1/4–1/3 times that of the compressive strength reported for dense alumina ceramics.

References

[1] Y. Hirata, Y. Terasawa, N. Matsunaga, S. Sameshima, Development of electrochemical cell with layered composite of the Gd-doped ceria/electronic conductor system for generation of H_2–CO fuel through oxidation–reduction of CH_4–CO_2 mixed gases, Ceramics International 35 (2009) 2023–2028.
[2] S. Matayoshi, Y. Hirata, S. Sameshima, N. Matsunaga, Y. Terasawa, Electrochemical reforming of CH_4–CO_2 gas using porous Gd-doped ceria electrolyte with Ni and Ru electrodes, Journal of the Ceramic Society of Japan 117 (11) (2009) 1147–1152.
[3] Y. Suga, R. Yoshinaga, N. Matsunaga, Y. Hirata, S. Sameshima, Electrochemical reforming of CH_4–CO_2 mixed gas using Gd-doped ceria porous electrolyte with Cu electrode, Ceramics International 38 (2012) 6713–6721.
[4] N. Yokunaga, Mechanical properties of porous material and its measurement, in: Y. Sugi, K. Tsutsumi, T. Nakata, Y. Nishimura, Y. Hujii (Eds.), Porous Materials—Characterization, Production and Application -, Fuji Technosystem Co., Tokyo, 1999, pp. 372–374.
[5] E. Ryshkewitch, Compression strength of porous sintered alumina and zirconia, Journal of the American Ceramic Society 36 (2) (1953) 65–68.
[6] D.J. Green, R. Brezny, C. Nader, The elastic behavior of partially-sintered materials, MRS Proceedings 119 (1988) 43, http://dx.doi.org/10.1557/PROC-119-43.
[7] D.J. Green, C. Nader, R. Brezny, The elastic behavior of partially-sintered alumina, in: C.A. Handwerker, J.E. Blendell, W. Kaysser (Eds.), Sintering of Advanced Ceramics, The American Ceramic Society, Westerville, OH, 1990, pp. 347–356.
[8] R.W. Rice, Comparison of physical property–porosity behavior with minimum solid area models, Journal of Materials Science 31 (6) (1996) 1509–1528.
[9] R. Cytermann, A new way to investigate the dependence of elastic moduli on the microstructure of porous materials, Powder Metallurgy International 19 (1987) 27–30.
[10] S.C. Nanjangud, D.J. Green, Mechanical behavior of porous glasses produced by sintering of spherical particles, Journal of the European Ceramic Society 15 (1995) 655–660.
[11] D. Hardy, D.J. Green, Mechanical properties of a partially sintered alumina, Journal of the European Ceramic Society 15 (1995) 769–775.
[12] Y. Hirata, Y. Tanaka, Pressure filtration model of ceramic nanoparticles, Journal of the American Ceramic Society 91 (3) (2008) 819–824.
[13] N. Matsunaga, Y. Nakashima, Y. Hirata, S. Sameshima, Rheology and pressure filtration of aqueous SiC suspensions of nanometer-sized bimodal particles, Ceramics International 36 (2010) 1581–1588.
[14] STC Corporation, Alumina (AL998, AL998E). Available from: ⟨http://www.ceramics.net/⟩ (accessed 1.07.13).